

Article

Dissolution Property of Serpentine Surface and the Effect on Particle–Particle Interaction Behavior in Solution

Zhihang Li ^{1,2}, Hongfei Cheng ^{1,*} , Yafeng Fu ^{3,*} , Kesheng Zuo ¹, Peng Gao ⁴ and Yuexin Han ⁴

¹ School of Earth Science and Resources, Chang'an University, Xi'an 710064, China; lizhihang@chd.edu.cn (Z.L.); keshengz@chd.edu.cn (K.Z.)

² The State Key Laboratory of Mineral Processing, BGRIMM Technology Group, Beijing 102200, China

³ Ansteel Beijing Research Institute Co., Ltd., Beijing 102200, China

⁴ School of Resources and Civil Engineering, Northeastern University, Shenyang 110004, China; gaopeng@mail.neu.edu.cn (P.G.); dongdafulong@mail.neu.edu.cn (Y.H.)

* Correspondence: h.cheng@chd.edu.cn (H.C.); fuyafeng110@126.com (Y.F.)

Abstract: The dissolution property of serpentine and its effect on the interaction between particles are reported here. Dissolution experiments showed that magnesium ions and hydroxyl were removed from the surface after mechanically stirring in solution, leading to the incongruent dissolution of ions. SEM, XPS, and Zeta potential analysis uncovered a significant change in serpentine surface potential and elements distribution after dissolution. Meanwhile, dramatic morphology changes on the surface were observed. A settlement test was carried out to explore the effect of dissolution on particle interaction. The results indicated that the settlement rate rises with increasing pH, but the fine particles had a lower settlement rate, showing the close connection between dissolution and particle interaction. AFM analysis revealed that the interparticle force could be changed because of surface properties at different pH values, leading to different interaction behaviors in the solution. In general, the adhesion force gradually increased and even changed from repulsive to attractive as pH ranged from 4 to 11, reflecting the adhesion behavior among particles in water. Moreover, compared to $-45 + 38 \mu\text{m}$ samples, $-38 \mu\text{m}$ particles are more likely to be kept repulsive in acid solution.

Keywords: serpentine; dissolution; surface morphology; particles interaction; AFM



Citation: Li, Z.; Cheng, H.; Fu, Y.; Zuo, K.; Gao, P.; Han, Y. Dissolution Property of Serpentine Surface and the Effect on Particle–Particle Interaction Behavior in Solution. *Minerals* **2023**, *13*, 799. <https://doi.org/10.3390/min13060799>

Academic Editor: Przemyslaw B. Kowalczyk

Received: 7 May 2023

Revised: 9 June 2023

Accepted: 10 June 2023

Published: 12 June 2023



Copyright: © 2023 by the authors. Licensee MDPI, Basel, Switzerland. This article is an open access article distributed under the terms and conditions of the Creative Commons Attribution (CC BY) license (<https://creativecommons.org/licenses/by/4.0/>).

1. Introduction

Serpentine is a magnesium-rich layered silicate mineral always associated with ascharite, pyrite, and pentlandite [1]. Because of the finely disseminated particle size and frangibility, it was prone to forming slime in grinding, leading to the deterioration of flotation performance [2,3]. Based on previous research, hydrophilic serpentine exhibited poor floatability, leading to a low flotation recovery [4,5]. Flotation is a worldwide used minerals separation technic based on the differences in physical and chemical properties of mineral surfaces [6–8]. In flotation, particle interaction is a very complicated process involving particle collision, adhesion, and desorption, which showed a close connection with the surface property. Previous literature has provided evidence that surface property has a profound influence on flotation performance [9–12]. As known to all, surface hydrophilicity and hydrophobicity reveal the floatability of minerals normally. However, pH, reagents, and ions could seriously change the surface property aiming to affect the flotation performance. For example, the surface charging property of chlorite could be changed by the adsorption of Cu^{2+} and Ca^{2+} on the surface, resulting in a decrease in reagent adsorbability to reduce the recovery [13]. Moreover, the hydrophilic quartz could be activated by Ca^{2+} , so an extremely high recovery was obtained in the plant and library [14]. On the contrary, the adsorption of Ca^{2+} on the quartz surface benefits the adhesion of oleate on the quartz surface, resulting in the difficulty in the flotation separation of cassiterite from quartz [15]. In alkaline conditions, serpentine floatability was elevated remarkably in the

presence of Cu^{2+} and Ni^{2+} , conducting to the beneficiation of serpentine in concentrate [16]. Furthermore, CMC and SHMP were widely used to strengthen the hydrophobicity by adsorption on the serpentine surface [3,4,17,18]. Moreover, the effects of particle surface morphology and roughness on surface potential were studied to reveal the close relationship between chemical property and physical structure [19–21]. Several studies have been carried out on the dissolution theory of sulfide, oxidized, and silicate minerals. The change in Zeta potential at different pH was analyzed [22–24]. All these studies mentioned above have confirmed that surface properties of minerals, such as surface morphology, surface components and elements distribution, are closely associated with physical characteristics.

In addition, the change in surface property not only influences the floatability of the mineral itself but also affects the particle–particle interaction behaviors [25–29]. It is considered that nanoscale forces dominate particle behavior in solution. For example, the adhesion of serpentine on pentlandite and chlorite surface could be eliminated by SHMP, and CMC was used to prevent the adsorption of serpentine on chromite and talc for improving the separation efficiency [14,30], which was caused by the change in interparticle force, the basic reason leading to the aggregation and dispersion occurred among multiple particles.

In recent years, AFM has been widely applied to study surface properties in many fields and could directly characterize and measure the nanoscale forces between particles [31,32]. For example, The attractive force between serpentine and ascharite could turn repulsive by adsorption of Ca^{2+} , Mg^{2+} , or Cu^{2+} on particles' surfaces, resulting in well dispersive flotation environment [33]. Cations could also change the repulsive force between kaolinite/montmorillonite and fine coal to be attractive [34]. By the way, the pH value also influenced particle interaction force, which changed from negative to positive with the increasing pH [35]. It is conspicuous that AFM plays a significant role in studying the particle mutual effect.

Although many studies focusing on the flotation performance of serpentine could be found, the study on its dissolution property is seldom reported. Meanwhile, we have never seen reports about the effect of dissolution property on particle interaction. Therefore, surface dissolution on serpentine is systematically investigated in this study, and SEM, XPS, and AFM are used to verify the intrinsic connection between surface property and particle interaction, which is helpful for the enrichment of dissolution theory and the interaction mechanism of silicate minerals.

2. Experimental Section

2.1. Samples

The sample used in this research was obtained from Xiuyan, Liaoning Province, China. After crushed and ground, samples were screened to $-45 + 38 \mu\text{m}$ and $-38 \mu\text{m}$. The chemical analysis is listed in Table 1, and the XRD result is displayed in Figure 1, indicating that the serpentine sample meets the test requirement with a purity of 96%. Particle size was also detected by Malvern Instruments Mastersizer (Mastersizer 2000, Malvern, England) analysis, as shown in Table 2.

Table 1. Chemical analysis results of serpentine and ascharite.

MgO	SiO ₂	B ₂ O ₃	Al ₂ O ₃	TFe	CaO	Ni
42.09	45.54	0.10	0.90	2.18	1.42	<0.1

Table 2. Results of particle size distribution of serpentine.

Particle Size	D ₁₀ /μm	D ₅₀ /μm	D ₉₀ /μm	Average Diameter/μm
−45 + 38 μm	17.7	33.4	47.8	42.5
−38 μm	2.1	11.0	42.3	12.8

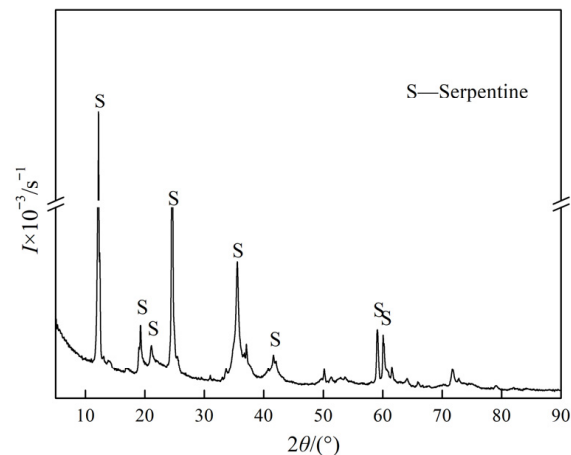


Figure 1. XRD spectrum of serpentine.

2.2. Experimental Methods

Dissolution experiments were carried out in a 30 mL flotation cell with a stirring speed of 1920 r/min. A total of 2 g serpentine sample was added to the cell with 20 mL deionized water, and a pH meter (pHS-3C, Leici, Shanghai, China) was used to detect the pH values of the solution. Once stirring had started, the pH values were recorded every 10 s until the end, when the pH remained unchanged. Then, the pulp was centrifuged for ICP analysis.

Settlement tests were carried out in a 200 mL measuring cylinder with a pulp concentration of 15 g/L. After stirring for 3 min using a magnetic stirring apparatus, 60 mL supernatant was separated 60 s later. Each test was repeated 3 times to ensure the accuracy of the results. Then, the supernatant and pulp that remained in the measuring cylinder were both dried and weighted to calculate the settlement rate, which reflected the dispersion situation of particles. The lower the settlement rate, the better the dispersion of particles. In this research, the result at pH of 4, 7, and 11 were studied. The solid weight in the supernatant is m , and that in the measuring cylinder is M . The settlement rate (η) can be expressed as follow:

$$\eta = m / (m + M) \quad (1)$$

2.3. Testing Methods

2.3.1. SEM Analysis

The change in surface property is directly reflected by the surface morphology. The particle surface microstructure was scanned by S5X-50 SEM-EDS (Shimadzu, Kyoto, Japan) analysis in this research to show the morphology change that occurred after dissolution.

2.3.2. Zeta Potential Analysis

Zeta potentials of serpentine at different pH were measured by Malvern Zetasizer Nano potential meter. Firstly, 20 mg of the sample with a particle size of less than 2 μm was added to 50 mL of deionized water. Potassium nitrate was used to maintain the ionic strength at 10^{-3} mol/L [36]. Then, the suspension was magnetically stirred for 10 min to make sure particles were well dispersed in the water. After that, the supernatant was measured using the potential meter 20 min later. All reagents used in this research are pure analytical grade. HCl and NaOH were used to adjust the pH values recorded by using a pHS-3C pH meter.

2.3.3. Atomic Force Microscope Analysis

The MFP-3D AFM (Bruker, Karlsruhe, Germany) is used to conduct all AFM experiments in this study. The surfaces of lumpy serpentine were polished to meet the requirements for AFM measurement at first. Then, slices were cut into pieces of $1 \times 1 \text{ cm}^2$ and used as substrates in the AFM test. Before use, these slices were cleaned by UV Ozone

Cleaner for 10 min and rinsed with a copious amount of deionized water, then dried with ultra-high purity N_2 gas. A standard liquid cell, cleaned by deionized water and dried with clean compressed air, was employed throughout the experiments [37]. The measurements were accomplished at pH of 4, 7, and 11. In this research, two boundary conditions are used: it is assumed either that the surface charges remain constant (constant charge) or that the surface potentials remain constant (constant potential), and interaction forces between particle and substrate were measured to approximately simulate the forces between two particles [38].

Triangular silicon nitride AFM probes with a spring constant of 0.15 N/m were used in the AFM experiments for force measurements. The spring constant was determined after all force measurements were made by using the thermal tuning method provided by Nanoscope 8.2 software. Serpentine particle suspension ($-45 + 38 \mu\text{m}$ and $-38 \mu\text{m}$) was dropped on a glass slide and dried in the air under an infrared lamp, respectively. A trace amount of epoxy adhesive was picked up by lowering a tipless AFM cantilever to touch the glass slide covered with epoxy adhesive [39,40]. Then, a serpentine particle was picked up by the tipless AFM cantilevers with epoxy adhesive. After that, the resulting assemblies were dried in clean air for at least 48 h. The colloidal probes were rinsed with ethanol and deionized water before being used. The force–distance curves were obtained by approaching and retracting the colloid probe against a desired substrate in aqueous water with preset pH values.

2.3.4. XPS Analysis

The XPS spectra were measured with an America Thermo VG ESCALAB250 spectrometer (ESCALAB250, Thermo Fisher Scientific, Waltham, MA, USA) using Al $K\alpha$ X-rays (1486.6 eV) as a sputtering source at a power of 150 W ($15 \text{ kV} \times 10 \text{ mA}$) to show elements composition on the serpentine surface. The measurements were performed inside the analysis chamber operating in a high vacuum of 5.0×10^{-7} Pa.

3. Results and Discussion

3.1. Dissolution of Serpentine in Solution

Surface property is a crucial factor that directly impacts flotation performance. Serpentine exhibited remarkable dissolving characteristics because the pulp always kept alkaline, which was considered to be related to dissolution. Then, systematical experiments were carried out to study the dissolution of serpentine samples with different particle sizes.

The results are shown in Figure 2. The pH of deionized water used in this study is about 6.0. After the addition of $-45 + 38 \mu\text{m}$ samples, the final pH of pulp was maintained at 8.5 after stirring for 100 s. The pH changed more rapidly after adding $-38 \mu\text{m}$ serpentine to deionized water and end up staying at approximately 9.1 as time extended to 60 s. The results revealed the fact that fine particles could dissolve after water leaching.

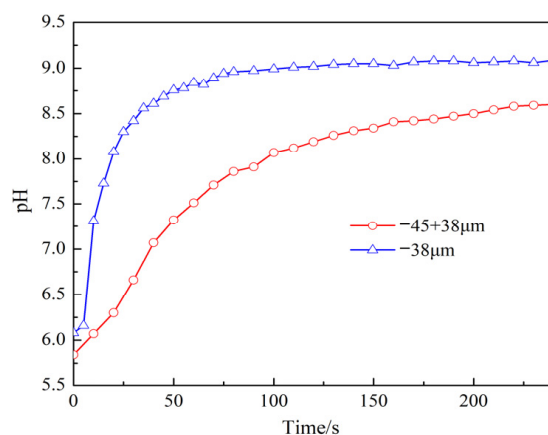


Figure 2. Curves of serpentine pH value changing with time.

For further understanding of the dissolution characteristics of serpentine, HCl was used to investigate the buffering ability of serpentine. The effect of HCl on solution pH is displayed in Figure 3. Without HCl, the pH was about 9.1, as discussed above, then it decreased to 6.81 after 4.0 mL HCl (mass fraction 0.2%) was added to the pulp, but it promptly decreased to 2.0 after 0.5 mL HCl solution was used in pure water. Therefore, serpentine dissolves in water and can continue dissolving to make the pulp remain alkaline.

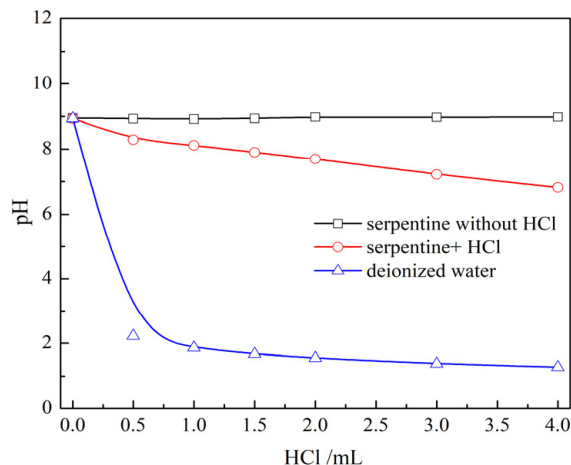


Figure 3. Effect of HCl dosage on pH of serpentine (−38 μm) pulp.

To explore the dissolved components from the surface, Mg²⁺ ions in the pulp were detected, as shown in Figure 4 (−38 μm serpentine used here). It showed that Mg²⁺ concentration increased with the usage of serpentine in a certain range, which confirmed the fact that a large number of Mg²⁺ in solution came from serpentine surfaces.

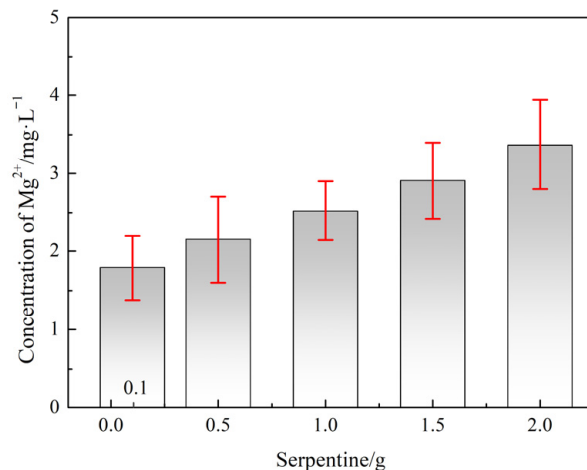


Figure 4. Effect of serpentine usage on Mg²⁺ concentration.

The effect of HCl on dissolution is shown in Figure 5. With the increase in HCl dosage, Mg²⁺ displayed a significant increase compared with data in Figure 4 without using HCl. It was proved that acid leaching could accelerate serpentine dissolution, and chemical reactions were supposed to occur during this process.

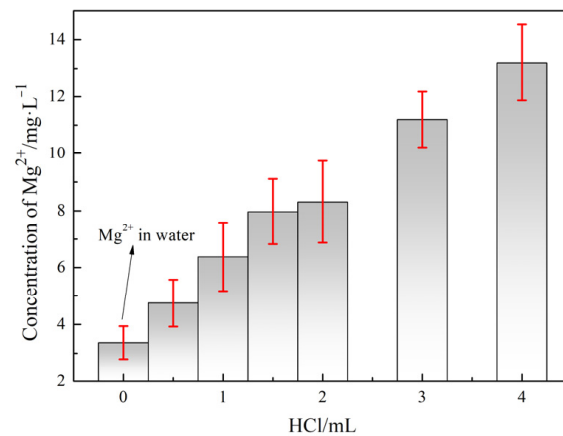


Figure 5. Effect of HCl dosage on Mg²⁺ concentration.

3.2. Serpentine Dissolution Characteristics on Surface

By invoking the assumption that the dissolution of various groups occurs on the surface, the components of serpentine surfaces treated by water/HCl were analyzed by XPS, and the elements' relative contents are listed in Table 3. The carbon concentrations were not necessarily representative of serpentine samples due to the air exposure of samples before analysis. The Mg²⁺ content was 21.97% on the original surface of the serpentine; then, it decreased to 18.65% after treatment in water. More Mg²⁺ was removed from the surface in an acid solution, and the content was further reduced to 16.72%. Therefore, the elements distribution on the serpentine surface could be changed in water or HCl solution.

Table 3. Surface elements relative content of serpentine.

Samples (−38 μm)	Elements/%			
	C	O	Mg	Si
Serpentine	8.76	53.69	21.97	15.61
Serpentine + H ₂ O	13.15	53.66	18.65	14.55
Serpentine + HCl	9.81	55.91	16.72	17.55

As lots of magnesium ions are removed from the surface, the surface potential is supposed to have a remarkable change in this condition. The Zeta potential as a function of pH is displayed in Figure 6, revealing that the point of zero charge (PZC) is 9.2 for serpentine without treatment, and the surface potential decreases after dissolving in pure water, as shown in the blue line. The PZC even further decreases to 3.6, where there are many H⁺ in water. It is apparent that more cations (Mg²⁺) dissolve from the surface compared to anions (−OH). Therefore, it is incongruent dissolution that leads to the decrease in Zeta potential.

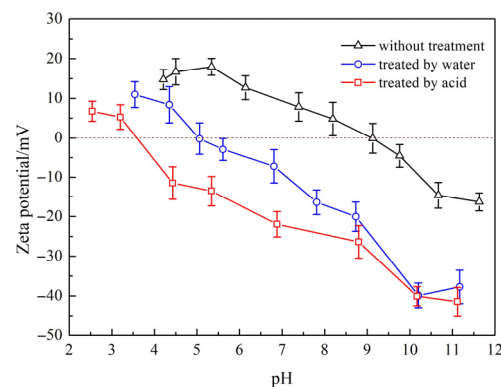


Figure 6. Zeta potential analysis of serpentine.

Because of the incongruent dissolution of magnesium with respect to hydroxyl, the surface structure is changed, which is scanned by SEM, as shown in Figure 7. The surface of the original sample was very smooth, and the sheet structure was observed in Figure 7a. After parts of the surface components dissolved in water, the smooth surface disappeared, and a nutty structure formed on surfaces, as shown in Figure 7b. After being treated by acid leaching, the original structure was destroyed by HCl, and then protruding structure covered the surface, as displayed in Figure 7c. It is certain that surface morphology was seriously affected by dissolution behaviors.

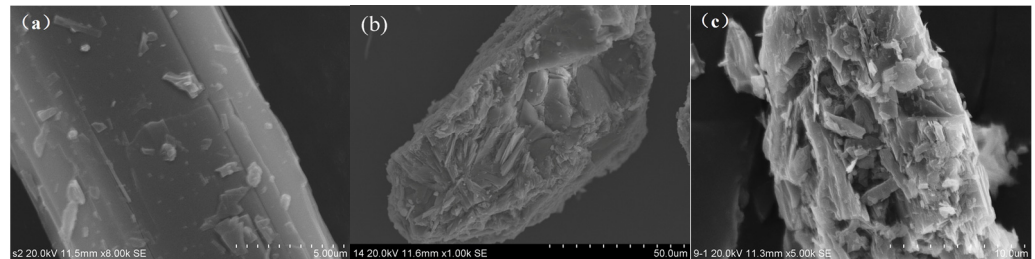
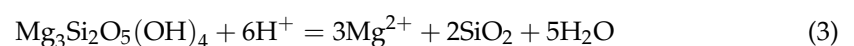
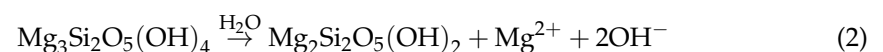


Figure 7. SEM images of serpentine surfaces treated in different solutions. (a) Original sample; (b) treated by water; (c) treated by HCl.

To uncover more details, AFM is also applied to measure the height change on mineral surfaces exposed to different solutions. The polished serpentine substrate without water/HCl treatments shown in Figure 8(a3) displays a smooth surface where only a difference of 4.3 nm in height is detected. However, obvious protrusions appeared on the partial region of the surface after being treated by water leaching. Compared with the smooth structure in Figure 8(a1), a part of the component on the surface dissolves in water, leading to the formation of protruding structure where a difference of approximately 13.3 nm in height is measured as shown in Figure 8(b3). After being treated with an HCl solution, the surface morphology had a more significant change, so the surface height changed by 30 nm, which was much larger than that in Figure 8(c3). Figure 8 shows that the original smooth surface was no longer observed, which has been replaced by corrugated structures. It confirmed that HCl accelerated the dissolution more apparently than that in water.

To provide deep sight into the dissolution property, the dissolution process is diagrammatically illustrated in Figure 9. Mg–O and Mg–OH are not solid bonds. Bond dissociation energies are approximately 394 kJ/mol and 238 kJ/mol, respectively. Therefore, lots of charged groups can dissolve into solution, especially free groups of HO–Mg–OH at position 1, which is most likely to move from surface to water. A small part of ions at position 2 is also included [41]. However, the Si–O bond dissociation energy is 798 kJ/mol, so silica tetrahedron has a stable structure and remains unchanged in water. In an acid solution, the –OH coming from the serpentine surface could react with H⁺, accelerating the surface dissolution process, then the groups connected to Si–O started to dissolve in large numbers. The dissolution reactions in water/HCl could be expressed as Equations (2) and (3) [1]:



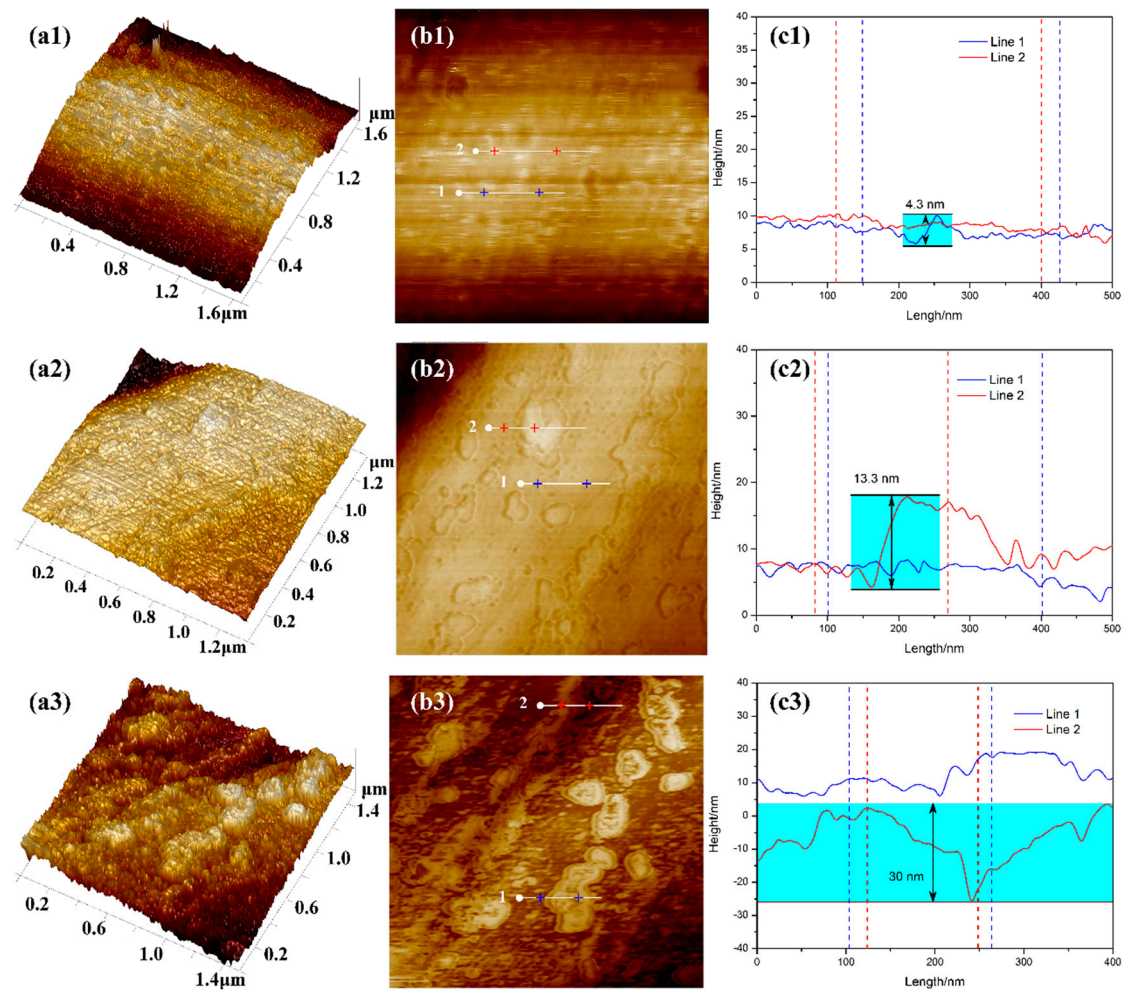


Figure 8. AFM images on the surface of samples ((a1): 3D image of raw ore; (a2): 2D image of raw ore; (a3): section height of raw ore; (b1): 3D image of sample dissolved in water; (b2): 2D image of sample dissolved in water; (b3): section height of sample dissolved in water; (c1): 3D image of sample dissolved in HCl; (c2): 2D image of sample dissolved in HCl; (c3): section height of sample dissolved in HCl).

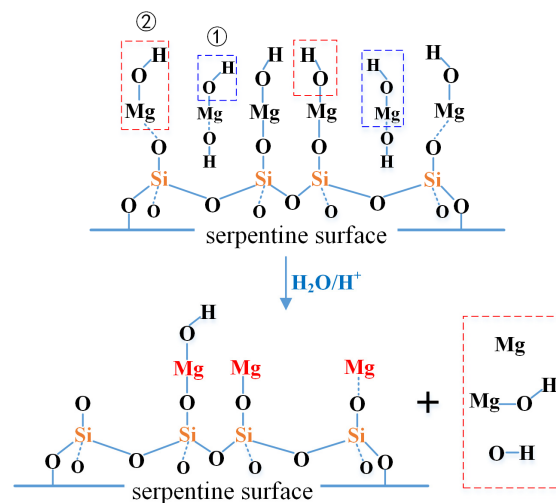


Figure 9. Dissolution process of serpentine on the surface.

3.3. Settlement Experiments of Serpentine Particles

It is certain that serpentine dissolution will lead to significant changes in surface morphology and surface potential, which are considered to influence particle interaction. So, settlement experiments were carried out, and settlement rates were calculated, listed in Table 4, revealing that the settlement rate increased with pH ranging from 4.1 to 10.9. For $-45 + 38 \mu\text{m}$ particles, the settlement rate is much higher than that of $-38 \mu\text{m}$ serpentine. Therefore, fine particles at low pH dispersed with each other, unveiling the different interaction behaviors in the solution.

Table 4. Results of settlement test at different pH values.

Particle Size	Settlement Rate/%		
	pH 4.1	pH 7.1	pH 10.9
$-45 + 38 \mu\text{m}$	87.5	91.7	98.1
$-38 \mu\text{m}$	56.2	61.3	74.8

3.4. Effect of Dissolution on Interparticle Force Measurements

As remarkable differences showed in settlement rates at different pH, it is supposed that particle interaction force plays a significant role in this process. Then, the forces between particles were measured. As shown in Figure 10a, adhesion forces were detected at pH of 4, 7, and 11 for $-45 + 38 \mu\text{m}$, which rise with increasing pH, causing particle adhesion and aggregation. Moreover, adhesion force at pH 11 was detected in a wide separation range within 100 nm, so dramatic particle adhesion occurred in this range compared with other conditions. Therefore, the force measurement result corresponded to the particle settlement rate above. In Figure 10b, the repulsive force (13.8 nN) was measured at pH 4 so that well dispersion occurred and the settlement rate was kept low, as listed in Table 4. However, the force at pH 7 (-7.5 nN) and 11 (-10.4 nN) was still attractive but not as large as the data displayed in Figure 10a, where the force was -16.2 nN and -19.7 nN at pH 7 and 9, respectively. Therefore, the fact that particle behavior turned from dispersion to adhesion as pH increased from 4 to 7 and 11 was unveiled. The same as Figure 10a, adhesion force at pH 11 worked in a wide range of particle separation, so a high settlement rate was obtained. The AFM result was in accordance with settlement tests, demonstrating the remarkable effects of pH on particle behaviors, and the opinion about the close connection of surface property with particle behavior is supported.

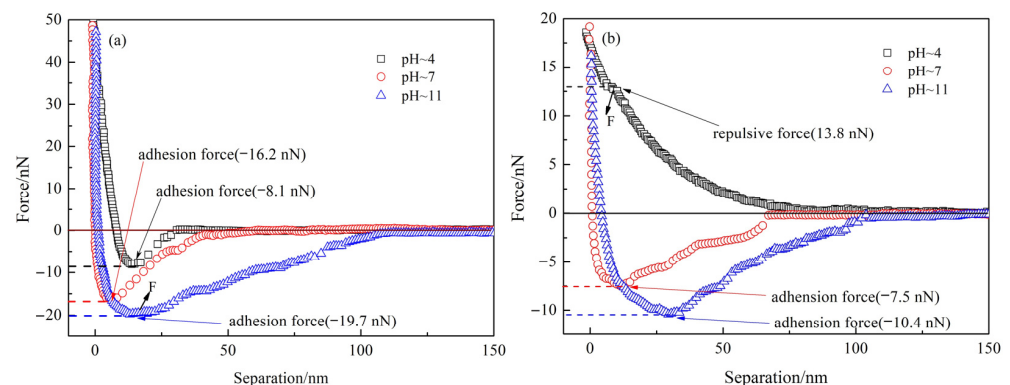


Figure 10. Force–distance curves for serpentine particle approaching serpentine substrate ((a), $-45 + 38 \mu\text{m}$; (b), $-38 \mu\text{m}$).

4. Conclusions

Serpentine dissolution property was systematically studied in this work, and the effect of dissolution on nanoparticle interaction was also discussed for the enrichment of dissolution theory and the interaction mechanism of serpentine particles.

1. Surface dissolution of serpentine caused a pH rise in the solution. As a result of the incongruent dissolution of magnesium with respect to hydroxyl, the surface potential was changed, and surface morphology was also altered. More cations dissolved from the serpentine surface compared with anions, leading to a sharp decrease in surface potential.
2. Particles dissolution had a significant effect on settlement rate, especially on $-38\ \mu\text{m}$ particles. After being treated with deionized water and acid, particles are more likely to well disperse in an acid solution. With the increase in pH from 4.1 to 10.9, particle dispersion was weakened, and the settlement rate increased apparently from 56.2% to 74.8%.
3. Surface properties, such as surface potential, morphology, and element distribution, were changed by component dissolution, which caused differences in interparticle forces, affecting the interaction behaviors in the solution. AFM results showed that the adhesion force between $-38\ \mu\text{m}$ particles was smaller and even changed from repulsive (13.8 nN) to attractive ($-10.4\ \text{nN}$) as pH ranging from 4 to 11. Therefore, serpentine particles are more likely to be kept repulsive in an acid solution, especially the $-38\ \mu\text{m}$ particles. The AFM results were in accordance with the results of settlement tests.

Author Contributions: Conceptualization, Z.L.; resources, H.C.; formal analysis, K.Z. and Y.F.; writing—original draft preparation, Z.L.; writing—review and editing, Z.L. and Y.F.; supervision, P.G. and Y.H. All authors have read and agreed to the published version of the manuscript.

Funding: The research leading to these results is funded by the Open Foundation of State Key Laboratory of Mineral Processing (BGRIMM-KJSKL-2023-04) and the National Natural Science Foundation of China (51804037).

Data Availability Statement: The data obtained and analyzed within the frame of this study will be made available by the corresponding author upon reasonable request.

Conflicts of Interest: The authors declare no conflict of interest.

References

1. Li, Z.H.; Han, Y.X.; Li, Y.J.; Gao, P. Surface Property of Serpentine. *J. Northeast. Univ.* **2018**, *39*, 404–408.
2. Lu, J.; Yuan, Z.; Liu, J.; Li, L.; Zhu, S. Effects of magnetite on magnetic coating behavior in pentlandite and serpentine system. *Miner. Eng.* **2015**, *72*, 115–120. [[CrossRef](#)]
3. Lu, Y.P.; Zhang, M.Q.; Feng, Q.M.; Long, T.; Ou, L.M.; Zhang, G.F. Effect of sodium hexametaphosphate on separation of serpentine from pyrite. *Trans. Nonferrous Met. Soc. China* **2011**, *21*, 208–213. [[CrossRef](#)]
4. Feng, B.; Feng, Q.; Lu, Y.; Gu, Y. The effect of PAX/CMC addition order on chlorite/pyrite separation. *Miner. Eng.* **2013**, *42*, 9–12. [[CrossRef](#)]
5. Feng, B.; Lu, Y.; Luo, X. The effect of quartz on the flotation of pyrite depressed by serpentine. *J. Mater. Res. Technol.* **2015**, *4*, 8–13. [[CrossRef](#)]
6. Guo, W.; Zhu, Y.; Han, Y.; Li, Y.; Yuan, S. Flotation performance and adsorption mechanism of a new collector 2-(carbamoylamino) lauric acid on quartz surface. *Miner. Eng.* **2020**, *153*, 106343. [[CrossRef](#)]
7. Li, X.; Liu, N.; Tang, L.; Zhang, J. Specific elevated adsorption and stability of cations in the interlayer compared with at the external surface of clay minerals. *Appl. Clay Sci.* **2020**, *198*, 105814. [[CrossRef](#)]
8. Yin, W.Z.; Wang, J.Z. Effects of particle size and particle interactions on scheelite flotation. *Trans. Nonferrous Met. Soc. China* **2014**, *24*, 3682–3687. [[CrossRef](#)]
9. Kozin, P.A.; Boily, J.F. Mineral surface charge development in mixed electrolyte solutions. *J. Colloid Interface Sci.* **2014**, *418*, 246–253. [[CrossRef](#)]
10. Liu, C.; Feng, Q.; Zhang, G. Electrokinetic and flotation behaviors of hemimorphite in the presence of sodium oleate. *Miner. Eng.* **2015**, *84*, 74–76. [[CrossRef](#)]
11. Farahat, M.; Hirajima, T.; Sasaki, K.; Doi, K. Adhesion of *Escherichia coli* onto quartz, hematite and corundum: Extended DLVO theory and flotation behavior. *Colloids Surf. B Biointerfaces* **2009**, *74*, 140–149. [[CrossRef](#)]
12. Cao, J.; Hu, X.Q.; Luo, Y.C.; Qi, L.; Xu, G.Q.; Xu, P.F. The role of some special ions in the flotation separation of pentlandite from lizardite. *Colloids Surf. A Physicochem. Eng. Asp.* **2016**, *490*, 173–181. [[CrossRef](#)]
13. Feng, Q.M.; Feng, B.; Lu, Y.P. Influence of copper ions and calcium ions on adsorption of CMC on chlorite. *Trans. Nonferrous Met. Soc. China* **2013**, *23*, 237–242. [[CrossRef](#)]

14. Luo, B.; Zhu, Y.; Sun, C.; Li, Y.; Han, Y. Flotation and adsorption of a new collector α -Bromodecanoic acid on quartz surface. *Miner. Eng.* **2015**, *77*, 86–92. [[CrossRef](#)]
15. Feng, Q.; Wen, S.; Zhao, W.; Chen, Y. Effect of calcium ions on adsorption of sodium oleate onto cassiterite and quartz surfaces and implications for their flotation separation. *Sep. Purif. Technol.* **2018**, *200*, 300–306. [[CrossRef](#)]
16. Cao, Z.; Zhang, Y.H.; Sun, C.Y.; Cao, Y.D. Activation mechanism of serpentine by Cu (II) and Ni (II) ions in copper-nickel sulfide ore flotation. *Chin. J. Nonferrous Met.* **2014**, *24*, 506–510. [[CrossRef](#)]
17. Li, Z.H.; Han, Y.X.; Li, Y.J.; Gao, P. Effect of serpentine and sodium hexametaphosphate on ascharite flotation. *Trans. Nonferrous Met. Soc. China* **2017**, *27*, 1841–1848. [[CrossRef](#)]
18. Feng, B.; Luo, X.P. The solution chemistry of carbonate and implications for pyrite flotation. *Miner. Eng.* **2013**, *53*, 181–183. [[CrossRef](#)]
19. Salmani Nuri, O.; Irannajad, M.; Mehdilo, A. Effect of surface dissolution on kinetic parameters in flotation of ilmenite from different gangue minerals. *Trans. Nonferrous Met. Soc. China* **2019**, *29*, 2615–2626. [[CrossRef](#)]
20. Boily, J.F.; Kozin, P.A. Particle morphological and roughness controls on mineral surface charge development. *Geochim. Cosmochim. Acta* **2014**, *141*, 567–578. [[CrossRef](#)]
21. Sinha, P.; Szilagyi, I.; Montes Ruiz-Cabello, F.J.; Maroni, P.; Borkovec, M. Attractive forces between charged colloidal particles induced by multivalent ions revealed by confronting aggregation and direct force measurements. *J. Phys. Chem. Lett.* **2013**, *4*, 648–652. [[CrossRef](#)] [[PubMed](#)]
22. Yin, X.; Gupta, V.; Du, H.; Wang, X.; Miller, J.D. Surface charge and wetting characteristics of layered silicate minerals. *Adv. Colloid Interface Sci.* **2012**, *179–182*, 43–50. [[CrossRef](#)] [[PubMed](#)]
23. Kusuma, A.M.; Liu, Q.; Zeng, H. Understanding interaction mechanisms between pentlandite and gangue minerals by zeta potential and surface force measurements. *Miner. Eng.* **2014**, *69*, 15–23. [[CrossRef](#)]
24. Li, Z.; Han, Y.; Zuo, K. Surface-charging and particles aggregation behavior of ascharite. *Physicochem. Probl. Miner. Process.* **2019**, *55*, 991–1001. [[CrossRef](#)]
25. Gui, X.; Xing, Y.; Rong, G.; Cao, Y.; Liu, J. Interaction forces between coal and kaolinite particles measured by atomic force microscopy. *Powder Technol.* **2016**, *301*, 349–355. [[CrossRef](#)]
26. Ozdemir, O.; Taran, E.; Hampton, M.A.; Karakashev, S.I.; Nguyen, A.V. Surface chemistry aspects of coal flotation in bore water. *Int. J. Miner. Process.* **2009**, *92*, 177–183. [[CrossRef](#)]
27. Wang, J.; Li, J.; Xie, L.; Shi, C.; Liu, Q.; Zeng, H. Interactions between elemental selenium and hydrophilic/hydrophobic surfaces: Direct force measurements using AFM. *Chem. Eng. J.* **2016**, *303*, 646–654. [[CrossRef](#)]
28. Kishimoto, S.; Kageshima, M.; Naitoh, Y.; Li, Y.J.; Sugawara, Y. Study of oxidized Cu(1 1 0) surface using noncontact atomic force microscopy. *Surf. Sci.* **2008**, *602*, 2175–2182. [[CrossRef](#)]
29. Obeid, S.; Guyomarç'h, F.; Francius, G.; Guillemin, H.; Wu, X.; Pezennec, S.; Famelart, M.H.; Cauty, C.; Gaucheron, F.; Lopez, C. The surface properties of milk fat globules govern their interactions with the caseins: Role of homogenization and pH probed by AFM force spectroscopy. *Colloids Surf. B Biointerfaces* **2019**, *182*, 110363. [[CrossRef](#)]
30. Bicak, O.; Ekmekci, Z.; Bradshaw, D.J.; Harris, P.J. Adsorption of guar gum and CMC on pyrite. *Miner. Eng.* **2007**, *20*, 996–1002. [[CrossRef](#)]
31. Butt, H.J. Measuring electrostatic, van der Waals, and hydration forces in electrolyte solutions with an atomic force microscope. *Biophys. J.* **1991**, *60*, 1438–1444. [[CrossRef](#)]
32. Butt, H.J.; Cappella, B.; Kappl, M. Force measurements with the atomic force microscope: Technique, interpretation and applications. *Surf. Sci. Rep.* **2005**, *59*, 1–152. [[CrossRef](#)]
33. Li, Z.; Han, Y.; Li, Y.; Gao, P. Interaction between mineral particles during ascharite flotation process and direct force measurement using AFM. *Physicochem. Probl. Miner. Process.* **2017**, *53*, 1161–1174. [[CrossRef](#)]
34. Xing, Y.; Xu, X.; Gui, X.; Cao, Y.; Xu, M. Effect of kaolinite and montmorillonite on fine coal flotation. *Fuel* **2017**, *195*, 284–289. [[CrossRef](#)]
35. Li, Z.; Han, Y.; Gao, P.; Wang, H.; Liu, J. The interaction among multiple charged particles induced by cations and direct force measurements by AFM. *Colloids Surf. A Physicochem. Eng. Asp.* **2020**, *589*, 124440. [[CrossRef](#)]
36. Crundwell, F.K. The mechanism of dissolution of minerals in acidic and alkaline solutions: Part v surfacecharge and zeta potential. *Hydrometallurgy* **2016**, *161*, 174–184. [[CrossRef](#)]
37. Leiro, J.A.; Torhola, M.; Laajalehto, K. The AFM method in studies of muscovite mica and galena surfaces. *J. Phys. Chem. Solids* **2017**, *100*, 40–44. [[CrossRef](#)]
38. Jiang, H.; Xie, Z.; Liu, G.; Yu, Y.; Zhang, D. Interaction forces between muscovite and silica surfaces in electrolyte solutions measured with AFM. *Trans. Nonferrous Met. Soc. China* **2013**, *23*, 1783–1788. [[CrossRef](#)]
39. Karamath, J.R.; Vallejo-Cardona, A.A.; Cerón-Camacho, R.; Zapata-Peñasco, I.N.; Garibay-Febles, V.; Aburto, J. Relative performance of several surfactants used for heavy crude oil emulsions as studied by AFM and force spectroscopy. *J. Pet. Sci. Eng.* **2015**, *135*, 652–659. [[CrossRef](#)]

40. Trefalt, G.; Ruiz-Cabello, F.J.M.; Borkovec, M. Interaction forces, heteroaggregation, and deposition involving charged colloidal particles. *J. Phys. Chem. B* **2014**, *118*, 6346–6355. [[CrossRef](#)]
41. Feng, B.; Lu, Y.P.; Feng, Q.M.; Ding, P.; Luo, N. Mechanisms of surface charge development of serpentine mineral. *Trans. Nonferrous Met. Soc. China* **2013**, *23*, 1123–1128. [[CrossRef](#)]

Disclaimer/Publisher’s Note: The statements, opinions and data contained in all publications are solely those of the individual author(s) and contributor(s) and not of MDPI and/or the editor(s). MDPI and/or the editor(s) disclaim responsibility for any injury to people or property resulting from any ideas, methods, instructions or products referred to in the content.